16 Physical Systems Biology and non-equilibrium Soft Matter

C.M. Aegerter, D. Assmann, G. Ghielmetti, U. Nienhaus, M. Schindlberger (Master Student), T. Schluck

in collaboration with: Institute of Molecular Life Sciences (K. Basler, T. Aegerter-Wilmsen, C. Lehner, S. Luschnig), ETH Zürich (E. Hafen, I. Sbalzarini, P. Koumoutsakos), EPF Lausanne (P. Renaud, D. Floreano), University of Lausanne (S. Bergmann), Biozentrum Basel (M. Affolter), University of Strasbourg (N. Rivier), University of Konstanz (G. Maret, W. Bührer, T. Sperling, N. Isert), New York University (C.C. Maass), Deutsches Luft- und Raumfahrtzentrum (M. Sperl), University of Twente (A. Mosk), Bulgarian Academy of Sciences (V. Petrov), Universite Joseph Fourier Grenoble (S. Skipetrov, F. Graner), Technion Haifa (E. Akkermans), University of Exeter (P. Vukusic), Yale University (A. Monteiro).

Work in the group of physical systems biology and non-equilibrium soft-matter is concerned with the study of developmental biology using physical techniques. In this, we are developing novel imaging techniques for the study of the influence of mechanical stresses on developmental processes. Moreover, the group works on the study of inherent non-equilibrium systems that can be tracked physically, such as driven granular gases. In the last year, we have made considerable progress in these two areas, where we have determined the elastic properties of developing wing disc tissues of the fruit fly Drosophila, as well as a description of the velocity distributions of granular gases in terms of kinetic theory, which is able to describe not only the driven steady state, but also the cooling state. These two projects will be described in detail below.

16.1 Photoelastic properties of Drosophila wing imaginal discs

In the study of developing tissues, we and others have put forward the idea that mechanical feedback can work as a regulatory mechanism in tissue growth [1–3]. In order to study this proposal experimentally, we have determined the photo-elastic properties of the wing disc tissue after the application of controlled forces while simultaneously determining its birefringence [4]. Unforced discs show a compression in the centre of the disc, as shown in Fig. 16.1, which increases with the age of the discs as they develop [5].

A schematic of the setup used to exert controlled forces onto the tissues is drawn in Fig. 16.2. The wing imaginal discs were attached to two separate cover slips using poly-lysine solution. This leads to an electrostatic attraction of the tissue with the cover slip and thus an efficient fixation. While one of these cover slips is fixed, the other is attached to a sheet of spring steel at a right angle. Due to the geometric measures and the bending stiffness of the spring sheet, a calibrated force can be exerted on the cover slip and hence the wing disc by bending the spring sheet. For this purpose we have used a translation stage capable of resolving movements down to a micron over a range of several mm.

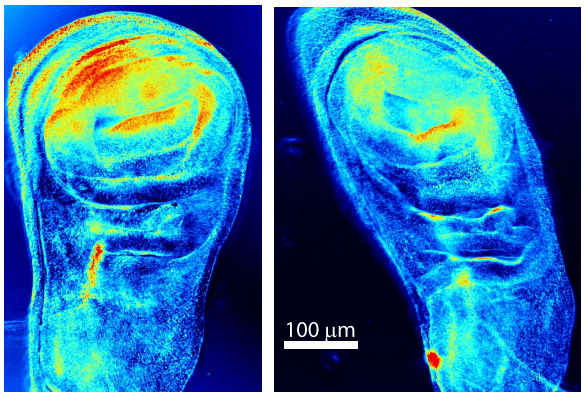

Fig. 16.1 – The retardance map of a wild type wing disc before (left) and after (right) uncontrolled stretching. The results are similar to those found previously on longer time scales and using a different setup. The colormap indicates retardance varying between 0 nm (black) and 10 nm (red) [6]. For a determination of photo-elastic properties, the stretching needs to be performed in a quantitative manner.

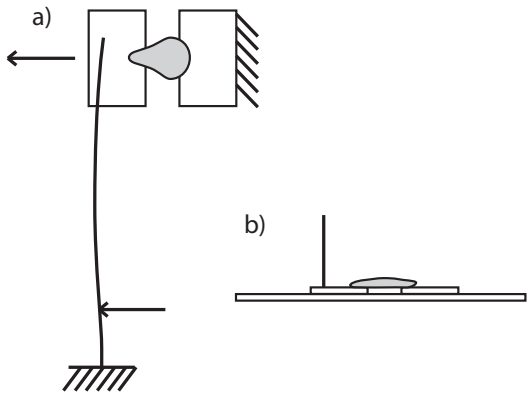

Fig. 16.2 – Top (a) and side (b) view of the mechanical forcing setup. The wing disc (grey) is attached to two glass cover slides, one of which is attached to a surface. The other cover slide is fixed to a spring sheet, which is forced by a translation stage at a given distance. This gives a controllable force ranging from 1μN to 1 mN, which is ideally suited to study epithelial tissues.

Given the point of contact of the translation stage with the spring sheet, we can easily calculate the force exerted on the wing disc from classical elasticity [8]:

$$F = \frac{6EI}{w^2(L-w)}d.$$

Here, $E = 2\times10^{11}$ Pa is the Young's modulus of the spring sheet, $I = a^3b/12$ is the area moment of inertia of the sheet with a thickness of $a = 50\mu$m and a width of $b = 1.1$cm. Furthermore, $L = 12$cm is the total length of the sheet and $w = 4$cm is the point of contact with the translation stage. Finally, d is the distance traveled by the translation stage. Taking these data on the spring sheet together yields a bending spring constant of 1.0 N/m, such that the setup is capable of exerting forces between 1μN and 1 mN.

Using the pulling setup described above, we have compressed and stretched wing discs with a controlled force exerted by the spring sheet. Typical results for different mechanical forcing are shown in Fig. 16.3. Here, the retardance map is somewhat different from the unattached discs, which could be due to the fact that the attachment with poly-lysine also exerts mechanical stresses locally. In the figure, three different stages of the experiment can be seen, corresponding to a compression of the wing disc with a force of 30 μN (top), a slight stretching (10 μN - middle) and strong stretching at 50 μN (bottom). We have averaged the retardance over the central area of the pulled disc tissue and find values of 2.9 nm in the compressed case, 2.5 nm in the marginally stretched case and 2.1 nm in the fully stretched case. In some of our experiments, the force of attachment on the cover slide was comparable to the force exerted by the spring sheet. This led to a detachment of the wing disc after having been subject to a stretching force for several minutes to half an hour. As can be seen from Fig. 16.4, such detached wing discs revert to their original size, which takes place over the course of 2-3 seconds. The slight difference in appearance visible in Fig. 16.4 is due to the fact that the unattached side of the disc can move in the z-direction bringing it

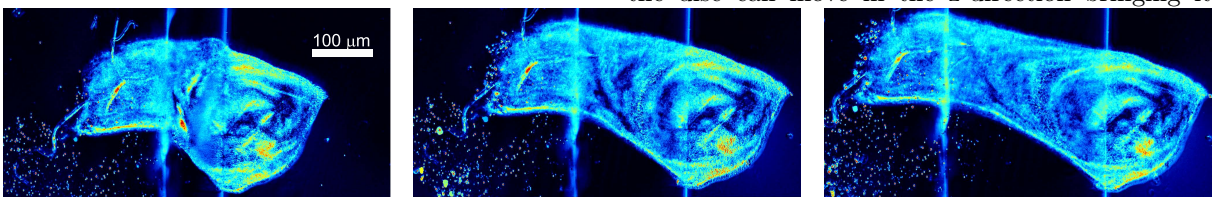

Fig. 16.3 – The retardance map of a wing disc at different levels of stretching in the y-direction. The colormap indicates retardance, changing from 0 nm (black) to 10 nm (red). In the left picture, the disc is compressed with a force of 30 μN, while in the middle the disc is roughly in its initial state with a stretching force of about 10 μN. The right picture shows a stretched wing disc at a force of 50 μN. Note that for an accurate determination of the changes in retardance, proper averages over the stretched tissues need to be taken. The resulting differences are of the order of 0.5 nm, with an increase in retardance for compressional stress and a decrease for tensional stress.

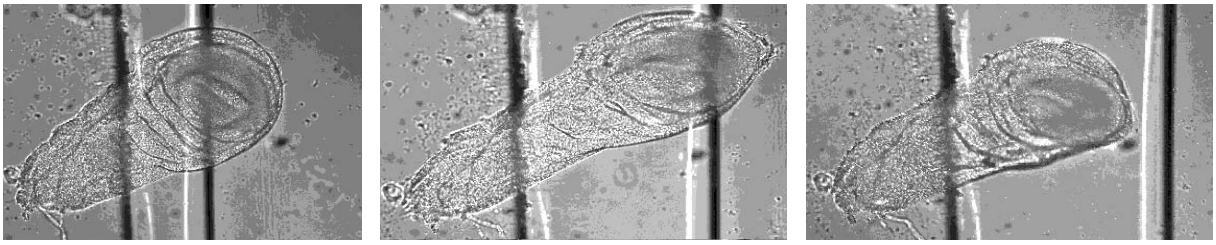

Fig. 16.4 – A stretched wing disc that has been detached from the cover slide (right). The disc reverted to its original shape and size before stretching (left) in spite of having been stretched substantially, (middle). The discrepancy in shape is explained by the fact that the unattached part of the disc is free to move in the z-direction thus losing the focus. This indicates that on the corresponding time scale of half an hour and for strains as big as 1, the disc behaves elastically.

out of focus and thus changing the form somewhat. This implies that on the time-scale of half an hour, the tissue does act elastically. In fact, a force extension curve of a typical wing disc is rather linear, as can be seen in Fig. 16.5, with an effective spring constant of 0.5(1)N/m. This directly corresponds to a Young's modulus of the order of 10^4 Pa.

In other developing tissues, which have been studied experimentally [7; 9; 10], spring constants of the order of 10^{-3} N/m were found. Thus it seems that the wing discs behave more stiff and elastic than other tissues. It should be noted, however, that these investigations were done on embryonic tissues, which is not the case for wing imaginal discs.

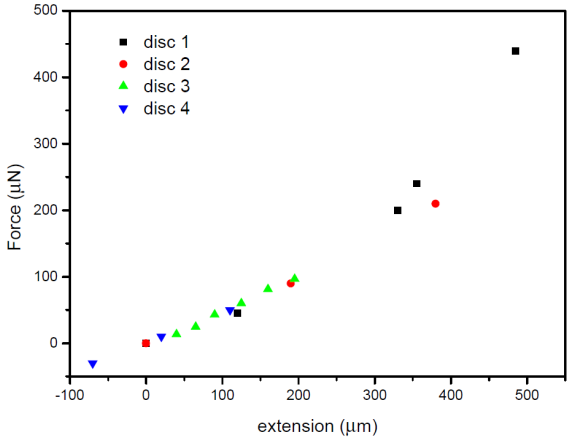

Fig. 16.5 – Force extension curves for four different wing imaginal discs. The extension is taken starting from the relaxed state. For a large range of extensions, the force needed is linear and only increases at strains in excess of 2. The initial slope of the curve implies a high spring constant of wing disc tissue as compared to embryonic samples [7; 9; 10].

For instance, the mechanical stresses in the larva when feeding and moving are much higher than in the embryo thus invoking stronger tissues. This is corroborated by moduli of adult tissues, such as blood vessels, skin or muscle, which range between 10^5 and 10^6 Pa [12; 13].

[1] T. Aegerter-Wilmsen, C.M. Aegerter, E. Hafen, and K. Basler, Mech. Develop. **124**, 318 (2007).

[2] B.I. Shraiman, Proc. Natl. Acad. Sci. USA. **102**, 3318 (2005).

[3] L. Hufnagel, A.A. Teleman, H. Rouault, S.M. Cohen, and B.I. Shraiman, Proc. Natl. Acad. Sci. USA. **104**, 3835 (2007).

[4] T. Schluck and C.M. Aegerter, Europ. Phys. J. **33**, 111 (2010).

[5] U. Nienhaus, T. Aegerter-Wilmsen, and C.M. Aegerter, Mech. Dev. **127**, 942 (2009).

[6] M. Shribak and R. Oldenbourg, App. Optics **42**, 3009 (2003); R.J. Wijngaarden, M.S. Welling, C.M. Aegerter, and K. Heek. NATO Science Series II: **142**, 61 (2004).

[7] R.A. Foty, C.M. Pfleger, G. Forgacs, and M.S. Steinberg, Development **122**, 1611 (1996).

[8] L.D. Landau and E.M. Lifshitz, Oxford (1960).

[9] E.M. Schötz, R.D. Burdine, F. Jülicher, M.S.

Steinberg, C.P. Heisenberg, and R.A. Foty, HFSP Journal **2**, 42 (2008).

[10] C. Wiebe and G.W. Brodland, J. of Biomechanics **38**, 2087 (2005).

[11] T. Aegerter-Wilmsen, A. Christen, E. Hafen, C.M. Aegerter, and K. Basler, Development **137**, 499 (2010).

[12] J.Zhou and Y.C. Fung, Proc. Nat. Ac. Sci. USA **94**, 14255 (1997).

[13] M.R. Neidert, E.S. Lee, T.R. Oegema, and R.T. Tranquillo, Biomaterials **23**, 3717 (2002).

16.2 Velocity distributions in levitated granular media

In collaboration with the University of Konstanz, we are studying the behaviour of granular gases using diamagnetic levitation [1]. Due to the levitation of the particles, it is possible to study the behaviour of the grains as a function of time when the excitation is switched off. Under normal circumstances, this behaviour is completely masked by the gravitational effect of grains falling to the bottom of the container. Due to the inelasticity of collisions between grains, the particles continually loose energy, which is a fundamental ingredient in the theoretical description of granular gases using kinetic theory [2]. This has led to a description of the freely cooling granular gas by Haff more than 25 years ago [3], which is used as a ground state in the description of excited granular gases [4].

Using a collection of monodisperse Bismuth shots, we have created a granular gas in the bore of a strong superconducting solenoid [5]. At an applied field of 13.5 T, the field gradient at the edge of the solenoid is strong enough such that the diamagnetic susceptibility of Bismuth leads to a repulsive force that equals gravity. Exciting the granular gas using an alternating component of the levitating field, a homogeneously driven granular gas can be created. This is different from usual granular gases, which are typically driven by mechanical shaking from the outside, which implies an inhomogeneous input of energy, which is difficult to calculate theoretically. For these differently excited granular gases, we can then determine the velocity distributions using particle identification and tracking given snapshots as those shown in Fig. 16.6. Here, deviations from the Maxwellian distribution are expected due to the non-equilibrium nature of the gas. This description will typically take place in the framework of kinetic theory, which in its simplest form will take the homogeneously cooling state as its starting point, which will be a scaling solution also for the steady state [6].

For a simple model, we will resort to the description of the homogeneous cooling state given in [5]. This implies that we will normalise the speeds by their mean, $c = v/\langle|v|\rangle$. For small speeds, it is then possible to calculate the velocity distribution

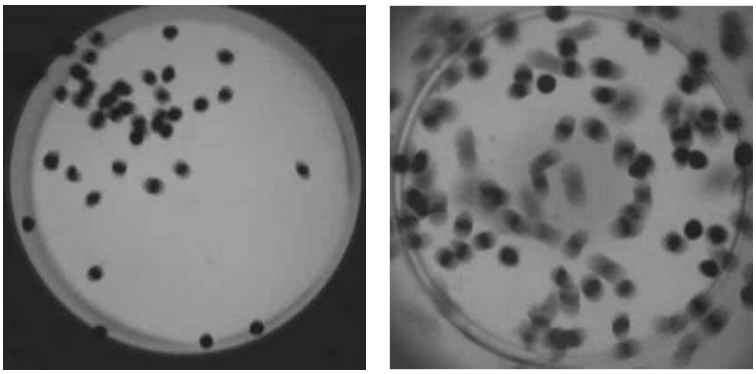

Fig. 16.6 – Snapshots of the distribution of particles during excitation using a magnet coil (left) and mechanically via a loudspeaker (right). In the first case the driving force is homogeneously distributed over the whole sample, whereas in the second case energy transfer takes place only at the boundary which results in a different distribution.

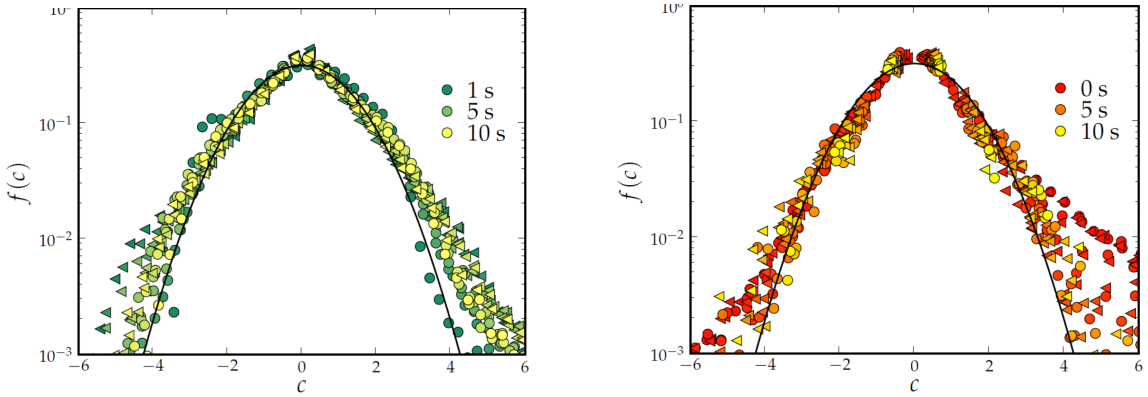

Fig. 16.7 – Velocity distributions for the different cases of driving (left: coil; right: speaker). The distributions are given for different time periods after which the driving has been switched off. This means that the cooling process is studied. In case kinetic theory can be used to describe the process, the distributions should only scale via their width, which decreases according to Haff's law. As can be seen, this is not the case for the driving with a speaker. Here the distribution at late times approaches that of the homogeneously driven case, which does scale with cooling time.

starting from the equilibrium case of a Gaussian distribution given by:

$$G(c) = \frac{1}{\pi} exp(-c^2/\pi).$$

The distribution $p(c)$ can then be treated by $\Delta(c) = p(c)/G(c) - 1$, corresponding to the first Sonine polynomial, assuming a normalised distribution with a mean speed of unity. For a full characterisation, we will finally have to determine $\langle c^2 \rangle$, which in the simplest description of the homogeneously cooling granular gas, can be achieved using the collisional dynamics of an average particle. With the loss of kinetic energy due to collisions one obtains:

$$\begin{aligned} 2\ell \frac{d\langle |v| \rangle}{dt} &= (1-\rho^2)\langle |v| \rangle^2 \\ &= \langle v^2 - \langle |v| \rangle^2 - \rho^2(\langle |v| \rangle - v)^2 \rangle \end{aligned}$$

for the rate of change in the speed of an average particle, where the first term corresponds to the dynamics implied by Haff's law. Here, ℓ is the mean free path of a particle between collisions and $(1-\rho^2)$ is the average coefficient of restitution. Solving this equation by taking into account that $\langle v \rangle = 0$, one obtains $\langle v^2 \rangle = 2\langle |v| \rangle^2$ or alternatively $\langle c^2 \rangle = 2$, independent of the coefficient of restitution. This implies for the velocity distribution:

$$p(c) = G(c)(\frac{2}{\pi})^3(\pi^2/2 - 5\pi/2c^2 + c^4).$$

We have now determined the velocity distributions during the cooling process in order to assess whether this state can be used as a ground state onto which the steady state properties scale. The different distributions for different excitations are shown in Fig. 16.7.

The velocity distribution at different times in the cooling process do scale with the temperature of the gas in the homogeneously excited case, as is predicted by kinetic theory. This however is not the case for a mechanically shaken gas, where the energy input is from a boundary. Interestingly, the coefficient of restitution does not seem to play a role in the description of the velocity distributions at small speeds, as the Sonine expansion we find is independent of the coefficient of restitution. This is corroborated from our data of particles at different $\rho = 0.35$ and $\rho = 0.7$, as well as the data of Reis *et al.* [7] with still higher $\rho = 0.95$. In addition, the data show conclusively that the deviations from near equilibrium distributions in most experiments [2] are mainly due to boundary effects implied by the excitation of the particles in these studies.

[1] W. Braunbek, Z. Phys. **121**, 764 (1939).

[2] J.S. Olafsen, and J.S. Urbach, Phys. Rev. Lett. **81**, 4369 (1998); Phys. Rev. E **60**, R2468 (1999); D.L. Blair, and A. Kudrolli, Phys. Rev. E **67**, 041301 (2003).

[3] P.K. Haff, J. Fluid. Mech. **134**, 401 (1983).

[4] X. Nie, E. Ben-Naim, and S. Chen, Phys. Rev. Lett. **89**, 204301 (2002).

[5] C.C. Maass, N. Isert, G. Maret, and C.M. Aegerter, Phys. Rev. Lett. **100**, 248001 (2008).

[6] J.M. Montanero and A. Santos, Gran. Mat. **2**, 53 (2000).

[7] P. Reis, R.A. Ingale and M.D. Shattuck, Phys. Rev. E **75**, 051311 (2007).